

Spin-Filtering Multiferroic-Semiconductor Heterojunctions

Na Sai,¹ Jaekwang Lee,¹ Craig J. Fennie,² and Alexander A. Demkov¹

¹*Department of Physics, The University of Texas at Austin, Texas, 78712*

²*Center for Nanoscale Materials, Argonne National Laboratory, Argonne, IL, 60439*

(Dated: August 24, 2007)

We report on the structural and electronic properties of the interface between the multiferroic oxide YMnO_3 and wide band-gap semiconductor GaN studied with the Hubbard-corrected local spin density approximation (LSDA+U) to density-functional theory (DFT). We find that the band offsets at the interface between antiferromagnetically ordered YMnO_3 and GaN are different for spin-up and spin-down states. This behavior is due to the spin splitting of the valence band induced by the interface. The energy barrier depends on the relative orientation of the electric polarization with respect to the polarization direction of the GaN substrate suggesting an opportunity to create magnetic tunnel junctions in this materials system.

Multiferroics are materials in which ferroelectricity and magnetism coexist in a single phase. Efforts have shifted from the question of “coexistence”, to identifying strategies that will increase the coupling between the two orderings. This increased functionality opens opportunities for novel electrically or magnetically controlled devices. One route that is promising for practical applications is to employ multiferroic thin films and multilayered structures, the properties of which can be readily manipulated at the nanoscale.^{1,2} Multiferroic YMnO_3 ^{3,4} is considered an attractive candidate for use in transistor devices because of its purity from volatiles such as Pb or Bi and its moderate dielectric constants.

Much effort has been directed at synthesizing and characterizing thin films of hexagonal YMnO_3 as a potential gate dielectric for semiconductor devices, e.g., YMnO_3 on Si(111)^{5,6,7,8}, on wurtzite GaN, or on ZnO^{9,10,11}. Despite the remarkable progress in synthesis, the role of the interface – strain, chemistry, etc., – on the ferroelectric and magnetic properties of YMnO_3 thin films is poorly understood and difficult to separate experimentally. In this Letter, we apply density-functional theory to calculate the electronic structure and band alignment at a realistic YMnO_3/GaN interface. We demonstrate that interfacial spins behave differently from those in the bulk. This interface effect leads to a spin splitting in the valence bands giving rise to different band offsets for spin up and down states. Intriguingly, the difference in the band offsets depends on the polarization direction of YMnO_3 relative to that of the polar GaN substrates, suggesting that the system could be utilized in spin-filtering tunneling junctions.

Bulk YMnO_3 and wurtzite GaN both have hexagonal symmetry. YMnO_3 is antiferromagnetic (AFM) and ferroelectric (FE) (space group $P6_3cm$) while GaN is polar but not FE. X-ray diffraction of YMnO_3 thin films deposited on GaN (0001) substrates suggests an in-plane rotation of 30° between the unit cell axes of YMnO_3 and GaN. For a coherent interface this implies that YMnO_3 is under a 10% in-plane compressive strain.^{9,10,11} This large epitaxial strain has been attributed by Posadas *et al.* to the energy gain from the interfacial bond formation.¹¹

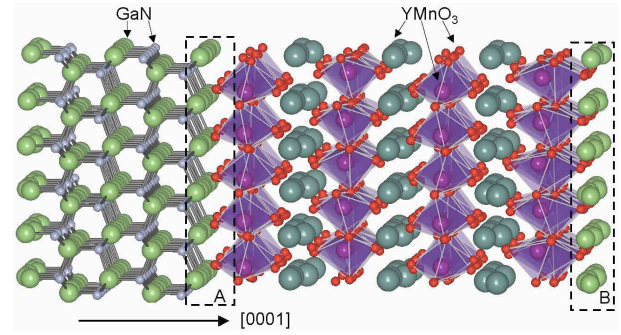


FIG. 1: The structural model of the YMnO_3 -GaN heterojunction. The two inequivalent interfaces viewed along (0001) and (000 $\bar{1}$) are defined as A and B, respectively.

Here, we adopt the experimentally determined interfacial relation and build heterostructures composed of two unit cells of YMnO_3 and GaN each, with a total of 24 atomic layers (Fig. 1). Both YMnO_3/GaN interfaces are comprised of Ga and apical oxygens, coming from YMnO_3 and GaN, respectively. The interfacial oxygens are placed above the *fcc* sites (*i.e.*, the threefold cavity sites) of the Ga surface. The periodic boundary condition in our calculations creates two inequivalent Ga-O bonded interfaces between the sequence of YMnO_3 and GaN, one with oxygens above the Ga (0001) face and another with oxygens above the Ga (000 $\bar{1}$) face (see interfaces A and B in Fig.1 respectively).

We perform DFT calculations of YMnO_3 within the LSDA+U approximation with $U = 6$ eV and $J = 0.9$ eV.¹² The value of U was extracted from experiment (XPS¹³). We obtain a band gap of 1.46 eV (1.47 eV)¹³ and lattice parameters of $a_{\text{YMO}} = 6.09\text{\AA}$ (6.127 \AA)¹⁵ and $c/a = 1.86$ (1.86) which agree well with experiment (shown in parentheses). The Mn spins were treated in a frustrated collinear-AFM approximation as the 120° non-collinear spin structure observed in bulk YMnO_3 is beyond the computational capabilities for the realistic interface that we consider here. For bulk GaN, we carried out LDA calculations and found $a_{\text{GaN}} = 3.15\text{\AA}$, $c/a = 1.627$, and $u = 0.377$. The LDA band gap is 2.1 eV, which is

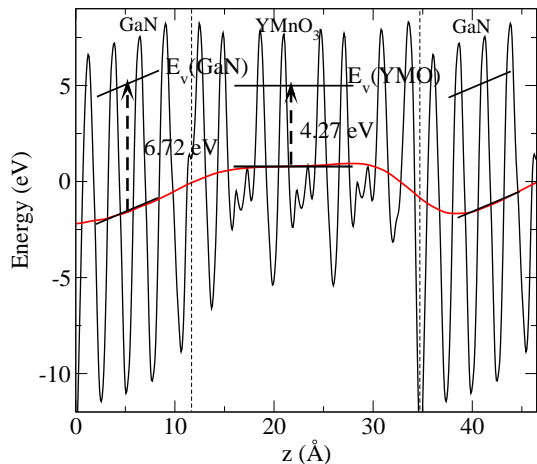


FIG. 2: The profile of the macroscopically averaged electrostatic potential across the $\text{YMnO}_3\text{-GaN}$ supercell P_1 . The straight lines are the top of the valence bands measured with respect to the average of the potential in each material, the values are referenced from independent bulk calculations.

below the true value 3.5 eV. Since the Hubbard correction does not provide genuine improvement in GaN, we used a Hubbard U only on the Mn atom.

To isolate the effect of strain, we first relax bulk YMnO_3 under in-plane compressive strain of $\sqrt{3}a_{\text{GaN}}/a_{\text{YMnO}_3} \sim 10\%$. The c -axis lattice parameter expands by $\sim 7\%$, consistent with Ref. 11. The Mn moments are slightly reduced $\sim 3.6\mu_B$ compared to the unstrained bulk value of $3.77\mu_B$. The distances between Mn and the in-plane oxygens Mn-O_P shorten to $\sim 1.86\text{\AA}$, while the distances between Mn and the apical oxygens Mn-O_A lengthen to $\sim 1.9\text{\AA}$, compared to $\sim 2.04\text{\AA}$ and $\sim 1.86\text{\AA}$, respectively, in the unstrained bulk. Despite the significant shortening of the Mn-O_P bonds, no changes occur to the topmost valence bands including $O_P p_{x,y}$ and Mn d_{xy} and $d_{x^2-y^2}$ orbitals as well as the unoccupied d_{z^2} states. The most noticeable change occurs in the $O_A p$ states and the $O_P p_z$ states immediately below the $O_P p_{x,y}$ bands, which downshift by ~ 0.6 eV near the Γ point, presumably due to strain-induced buckling of MnO_5 bipyramids.

Because wurtzite GaN is polar (a permanent dipole moment is produced by each bilayer of Ga^+ and N^-) we construct two supercells; “ P_1 ” with the FE polarization in YMnO_3 pointing along GaN (000 $\bar{1}$), and “ P_2 ” with the FE polarization pointing along GaN (0001). We then relax both supercells fixing the in-plane lattice constant to a_{GaN} . In either supercell, the vertical distances between the apical oxygens and the Ga atoms at the A and B interfaces (see Fig.1) are drastically different, ranging from 1.1–1.2 \AA at interface A to 0.2–0.6 \AA at interface B . The different bonding structures of two interfaces agrees with the behavior of oxygen adatoms adsorbed on Ga surfaces in the low oxygen coverage (growth) condition of GaN.¹⁶

Fig. 2 shows the macroscopically averaged electro-

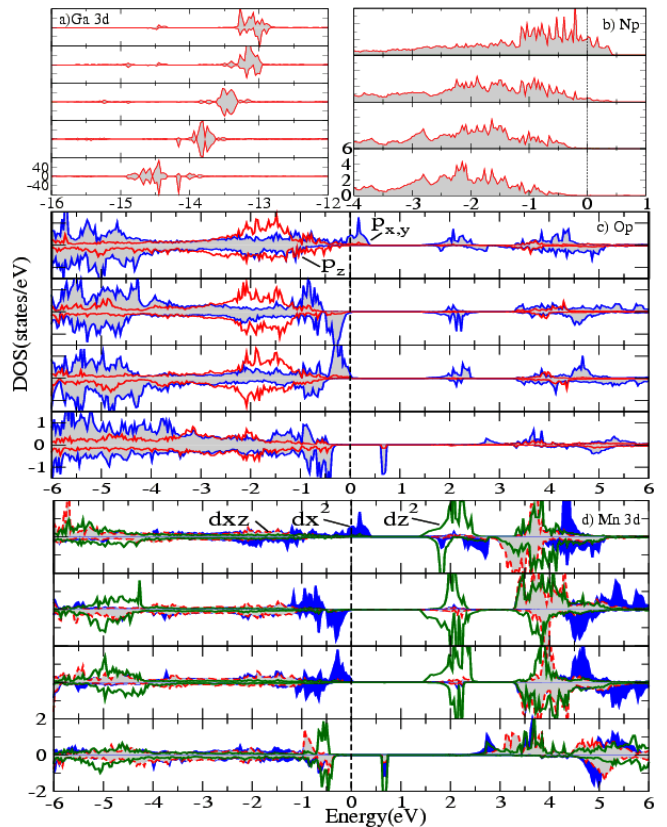


FIG. 3: Orbital-resolved DOS projected on atomic layers of the $\text{YMnO}_3\text{-GaN}$ supercell shown in Fig. 1. In each panel, the top and bottom most graph corresponds to interface A and B , respectively. The projected DOS of Mn d_{xy} and d_{yz} (not shown) are nearly degenerate with d_{x^2} and d_{xz} respectively shown in d). The vertical lines mark the Fermi level.

static potential the z direction. The polarization field in GaN, evident from the slope of the electrostatic potential, induces charge transfer across the film and induces screening on the opposite sides of the GaN films. As a consequence, the residual field across YMnO_3 , parallel (antiparallel) to the field in GaN in supercell P_1 (P_2), is small. Using the effective ionic charges,⁴ we estimate the polarizations of YMnO_3 in the supercell to be $-9.99\mu\text{C}/\text{cm}^2$ for P_1 and $8.43\mu\text{C}/\text{cm}^2$ for P_2 . These numbers are slightly lower than $14.0\mu\text{C}/\text{cm}^2$ calculated for the constrained bulk ($P \sim 8.8\mu\text{C}/\text{cm}^2$ in unconstrained bulk)⁴, indicating incomplete screening of the polarization charges at the interfaces. The polarization fields in these systems complicate comparison of the band edges directly from the lineup of the average potential as shown in Fig. 2

To analyze the electronic structure of the supercells we calculate the orbital-resolved, layer-projected density of states (PDOS). In the P_1 supercell, there is clearly a band bending of ~ 1 eV in GaN due to polarization, as illustrated by the deep Ga 3d valence states in Fig. 3a. The band bending is also evident in the topmost valence bands N_p in Fig. 3b that produces an upward bending

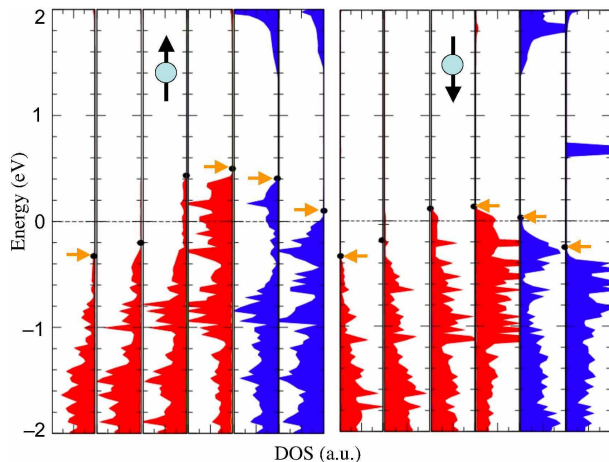


FIG. 4: Projected DOS of the YMnO₃-GaN P_1 supercell into 4 bilayers of GaN (red) and 2 unit-cells of YMnO₃ (blue). The left and right panels are DOS for spin-up and spin-down components. The black dots mark the valence band edge and the arrows mark the interface band edge.

at interface A and a downward bending at interface B , consistent with the experiments in GaN (0001) films.¹⁷ Despite this bending, there is no sign of gap closing as the thickness of our GaN films is much below critical.¹⁸ Fig. 3c and d show the DOS for Mn $3d$ and planar O_P $2p$ states. The interior layers look similar to the bulk layers, suggesting that the interior region converges to the bulk. The hole states at interface A are composed of Mn d_{xy}^\uparrow , $d_{x^2-y^2}^\uparrow$, O_P $p_{x,y}^\uparrow$ and a small contribution from O_A $p_{x,y}^\uparrow$. At interface B we observe a down shift in energy of the Mn $3dz^2$ orbitals (located at $\sim 2\text{eV}$ above E_F in the bulk), and a strong overlap with the O_p states. We encounter similar behavior in supercell P_2 except that the E_F is ~ 0.2 eV deeper than in P_1 . The difference can be related to charge compensation at the interfaces: in P_1 , the polarizations of YMnO₃ and GaN create opposite screening charges that partially cancel at the interfaces, while in P_2 , the polarizations create screening charges of the same sign and thus lead to higher accumulation than in P_1 .

In both supercells we observe that the spin moments of Mn at the YMnO₃/GaN interfaces deviate from their bulk values. On average the moment of Mn reduces to $\sim 3.3\mu_B$ at interface A and increases to $\sim 4.2\mu_B$ at interface B , producing a small net magnetization of $1.5\mu_B$ per supercell. This can be understood from the DOS analysis which shows a depletion of charge on the Mn d_{xy} and d_{x^2} at interface A and accumulation of charges on the Mn d_{z^2} orbitals at interface B . It is certainly possible that the precise route to the observed ferrimagnetic moment depends on the collinear approximation used in this study, but the basic physics of spin manipulation at the YMnO₃/GaN interface should be qualitatively similar if noncollinear spins are considered.

To calculate the band offset at the YMnO₃/GaN inter-

face, we project the spin-resolved DOS of the supercell onto unit cells of YMnO₃ and bilayers of the GaN as shown in Fig. 4, and calculated the band offsets for both the spin-up and spin-down components. In the case of P_1 , the valence band offset (VBO) is -0.05 eV for the spin-up component and -0.1 eV for the spin-down component at interface A , whereas a VBO is $+0.35$ eV for the spin-up and $+0.15$ eV for the spin-down at interface B (“+” and “-” represent upward and downward offsets going from GaN to YMnO₃). The band offset at both interfaces shows spin dependence. In particular, the spin-up electrons experience a potential higher by 0.2 eV than the spin-down electrons across interface B . This suggests that electrons of different spin directions experience different electrostatic scattering probabilities and that *spin-dependent barriers* can be produced in AFM multiferroic/semiconductor heterostructures. This effect is associated with spin splitting at the top of the valence bands. Recently, BiMnO₃ tunnel barriers were shown to be potential spin filters in magnetic tunnel junctions.¹⁹ But FM multiferroics such as BiMnO₃ are rare. Thus our observation of spin-dependent barriers in AFM multiferroic/semiconductor junctions might enable the use of a larger group of multiferroics with AFM orderings as spin filtering devices.

In the supercell P_2 (not shown), we find a VBO of 0.1 eV for the spin-up and -0.1 eV for the spin-down at interface A , similar to that of P_1 . At interfaces B , the VBO is $+0.2$ eV for spin-up and $+0.4$ eV for spin-down, slightly higher in amplitude than that of P_1 . It is noteworthy that the offset of the P_2 structure is reversed for up and down spins from that in P_1 at interface B , which suggests a possibility of controlling the spin scattering by a reversal of the ferroelectric polarization in YMnO₃. A small energy difference of ~ 20 meV is found in bulk YMO₃ when the spins are switched from the collinear to noncollinear in-plane configurations.²⁰ This is much less than the barrier differences we found between the up and down spins. Thus the magnetic anisotropy should not influence the spin-dependent effect we observe.

In conclusion, we report the details of the electronic structure of hexagonal YMnO₃-GaN heterojunctions. We consider two inequivalent Ga-O terminated interfaces that can be found in YMnO₃ films grown on (0001) and (000 $\bar{1}$) oriented GaN substrates and two possible orientations of the YMnO₃ polarization with respect to that of the GaN substrate. We find different band offsets for spin-up and spin-down components, with a larger variance at the (000 $\bar{1}$) interface. The spin-dependent interface barriers suggest that these heterostructures may be applicable in spin filtering tunneling devices. Our results are relevant not only to YMO films but also to other multiferroic thin films with coexisting antiferromagnetic and ferroelectric structures.

This work is supported by the Office of Naval Research under grant N000 14-06-1-0362 and Texas Advanced Computing Center.

-
- ¹ R. Ramesh and N. A. Spaldin, *Nature Materials*, **6**, 21 (2007).
- ² W. Prellier, M. P. Singh, and P. Murugavel, *J. Phys. Cond. Matt.* **17**, 803 (2005).
- ³ C.J. Fennie and K.M Rabe, *Phys. Rev. B* **72**, 100103 (2005).
- ⁴ B. B. van Aken, T. T. M. Palstra, A. Filippetti, and N.A. Spaldin, *Nature Materials* **3**, 164 (2004).
- ⁵ N. Fujimura, T. Ishida, T. Yoshimura, and T. Ito, *Appl. Phys. Lett.* **69**, 1011 (1996).
- ⁶ N. Fujimura *et al.*, *J. Appl. Phys.* **80**, 7084 (1996).
- ⁷ T. Yoshimura, N. Fujimura, and T. Ito, *Appl. Phys. Lett.* **74**, 414 (1998).
- ⁸ W.-C. Yi *et al.*, *Appl. Phys. Lett.* **73**, 903 (1998).
- ⁹ K.-R. Balasubramanian *et al.*, *Thin Solid Films* **515**, 1807 (2006).
- ¹⁰ Y. Chye *et al.*, *Appl. Phys. Lett.* **88**, 2903 (2006).
- ¹¹ A. Posadas *et al.*, *Appl. Phys. Lett.* **87**, 1915 (2005).
- ¹² We have performed the LDA+U calculations using the Vienna Ab initio Simulation Package (VASP) with projector augmented wave potentials, a cutoff energy of 500 eV, and a Monkhorst-Pack Γ -centered $4 \times 4 \times 2$ k -points mesh for the bulk and supercell calculations. The supercell DOS was generated with a denser $6 \times 6 \times 4$ mesh. The forces from ionic relaxation of the supercells are $< 8\text{meV}/\text{\AA}$.
- ¹³ J.-S. Kang *et al.*, *Phys. Rev. B* **71**, 092405 (2005).
- ¹⁴ J.E. Medvedeva *et al.*, *J. Phys. Cond. Matt.* **12**, 4947 (2000).
- ¹⁵ B.B. van Aken, A. Meetsma, and T.T. M. Palstra, *Acta Crys. Sec. C* **57**, 230 (2001).
- ¹⁶ T.J. Zywietz, J. Neugebauer, and M. Scheffler, *Appl. Phys. Lett.* **74**, 1695 (1999).
- ¹⁷ S. Chevtchenko *et al.*, *Appl. Phys. Lett.* **88**, 2104 (2006).
- ¹⁸ V. Fiorentini *et al.*, *Phys. Rev. B* **60**, 8849 (1999).
- ¹⁹ M. Gajek *et al.*, *Nature Materials* **6**, 296 (2007).
- ²⁰ Fiebig *et al.*, *J. Mag. MAg. Mat.* **290**, 883 (2005).